Poly(vinyl chloride)/Kaolinite Nanocomposites: Characterization and Thermal and Optical Properties

Yasemin Turhan, Mehmet Doğan,* and Mahir Alkan

Department of Chemistry, Faculty of Science and Literature, Balikesir University, 10145 Balýkesir, Turkey

Nanocomposites of poly(vinyl chloride) (PVC) have been prepared by solution intercalation method using both natural and modified kaolinites. Kaolinite was modified with dimethyl sulfoxide (DMSO) to expand the interlayer basal spacing. The characterization of PVC/kaolinite nanocomposites was made by X-ray diffraction (XRD) and transmission electron microscopy (TEM); the interactions between kaolinite and PVC was discussed by FTIR-ATR; the thermal stability was determined by simultaneous DTA/TG. FTIR-ATR confirms hydrogen bonds formed between dimethyl sulfoxide molecules and the inner surface hydroxyl groups of kaolinite. XRD and TEM results give evidence that kaolinite was dramatically intercalated into nanoscale and homogenously dispersed in the PVC matrix. Thermogravimetric analysis indicated that introduction of clay to the polymer network resulted in an increase in thermal stability. Ultraviolet (UV) absorbance experiments showed that nanocomposites have a higher UV transmission than PVC film. The Kissinger method was used for calculation the decomposition activation energy. The results have shown that activation energy values at both stages for PVC/kaolinite nanocomposite are higher than those of pure PVC, indicating that addition of kaolinite particles improves thermal stability of PVC.

1. Introduction

The synthesis and characterization of new and novel materials are one of the main objectives of advanced material research. Polymer composites represent an important class of these types of materials. The properties of composite materials are greatly influenced by the degree of mixing between the two phases. In conventionally filled polymers, the constituents are immiscible, resulting in a coarsely blended macrocomposite with chemically distinct phases. This results in poor physical attraction between the organic and inorganic components, leading to agglomeration of the latter, and therefore, weaker materials. In addition, the micrometer-sized particles act as stress concentrators.[1,2] Recently, polymer nanocomposites, especially polymer-layered silicate nanocomposites, have become a valuable alternative to conventionally filled polymers and are of current interest because of the fundamental questions they address and their potential technological applications.[3−5]

Nanocomposites are a combination of two or more phases containing different compositions or structures, where at least one of the phases is in the nanoscale regime. These materials exhibit different behavior from conventional composite materials with microscale structure, due to the small size of the structural unit, their higher surface area, the high surface-to-volume ratio, and improved adhesion between nanoparticles and polymer.[1] The study of the formation of nanocomposites has been a very active area of research because very small amounts of clay bring about a large enhancement of the mechanical, thermal, electrical, optic and fire properties, and gas permeability as compared to their macro- and microcounterparts. Okada et al. have demonstrated that nylon−6-clay hybrids exhibit substantial improvements in mechanical, thermal, and rheological properties, making possible new material applications of the nylon polymer.[6,7] Benlikaya et al. prepared poly(ethyl methacrylate) (PEMA) and poly(2-hydroxyethyl methacrylate) (PHEMA) nanocomposites with sepiolite and its silylated form using the solution blend method, and found that the increase in thermal stability of nanocomposites for PEMA was higher than that of PHEMA because of weakening hydrogen bonds in PHEMA in the presence of sepiolite and modified sepiolite in polymer matrix; that the T_g temperatures of PEMA and PHEMA increased by adding of sepiolite and modified sepiolite; and that modification of sepiolite with APTS had a slight influence on thermal properties of the nanocomposites.[8]

In general, polymer nanocomposites are obtained by the dispersion of inorganic or organic nanoparticles into polymer matrix. Clays, which can interact with organic compounds by different mechanisms, are commonly used as additives because they are composed of layered silicates that can intercalate organic molecules.[1] The clay consists of stacked aluminosilicate layers that can be separated, but the clay layers, which are held together by electrostatic forces, cannot be broken into separate layers by simple shear. Thus, organic modification of the clay is necessary to achieve the separation of the stacked clay layers.[6,9] Usually the clay minerals are treated with different coupling agents in order to improve the compatibility of the clay minerals and the polymeric materials.[10] Different methods have been used such as in situ polymerization, melt-blending, and solution intercalation in the preparation of nanocomposites as described in the literature. The solution intercalation method for the preparation of polymer/clay nanocomposites is a very good method to obtain good nanodispersion of the clay in a polymer matrix.[6]

Polyvinyl chloride (PVC), as a commodity thermoplastic, has been widely used in industrial fields for many years. It has many good properties, such as low flammability, low cost, and formulating versatility, but the properties such as its poor impact toughness and low heat-softening temperature limit its application. Therefore, the thermal stability studies are of vital importance to the users of PVC. Rubber is widely used to toughen PVC composites. Again, a variety of elastomers have been developed to improve the impact toughness of PVC.[11] However, they often lead to reduction in strength, heat resistance modulus, and difficult processing of polymeric composites. Since rigid filler particles have been used to toughen PVC, great

* To whom correspondence should be addressed. E-mail: mdogan@balikesir.edu.tr. Fax: +90 266 612 12 15. Tel.: +90 266 612 10 00.

10.1021/ie901384x
Published on Web 01/07/2010

progress has been made. In addition to toughening PVC with rigid filler particles, researchers can decrease cost, and good mechanical properties, thermal stability, and processing properties are simultaneously obtained.[12] In recent years, various nanoscale fillers, including montmorillonite, calcium carbonate, aluminum oxide, and silica have usually been reported.[13] The study of polymer/clay nanocomposites offers a novel approach in the preparation of high performance PVC nanocomposites. However, little attention has been given to PVC nanocomposites that are prepared via the solution intercalation method. Up to date, only a few publications about PVC/clay nanocomposites have been reported, and the fine nanostructures of resultant nanocomposites are scarcely obtained. Wan et al. used Na^+-MMT and two organically modified MMTs to prepare polyvinyl chloride (PVC)/montmorillonite (MMT) nanocomposites by melt blending. These nanocomposites were found with partially intercalated structure, enhanced mechanical properties, and improved processing stability.[14] Vandevyver and Eichholz synthesed PVC/Na-bentonite nanocomposites via in-situ polymerization with the exfoliation of Na-bentonite in water and found that nanocomposites have useful properties in PVC paste applications, exhibiting shear thinning rheology, improved thermal stability, and transparency.[15] Wang and co-workers also prepared PVC/MMT nanocomposites with immiscible and intercalated structures by melt blending, and studied the thermal properties and mechanical properties of the nanocomposites in the presence and absence of DOP.[16−18] To the best of our knowledge, there is no report related to the PVC/kaolinite nanocomposite. Kaolinite is a 1:1 dioctahedral aluminosilicate that has two different basal cleavages faces. One basal face consists of a tetrahedral siloxane surface. The other basal surface consists of an octahedral gibbsite sheet. Both of these surfaces are theoretically electrically neutral. At the edges of a 1:1 layer, the structure is disrupted and broken bonds occur that are accommodated as OH groups. These edges are estimated to occupy approximately 10% of the whole kaolinite surface. Kaolinite has a wide variety of applications in industry, particularly as paper filler and coating pigments. It is used as an extender in water-based paints and ink, as a functional additive in polymers, and is a major component of ceramics. Kaolinite is an inexpensive additive that can improve the properties of the material.[19] In this study, we synthesed nanocomposites with different relative compositions based on PVC and both natural and modified kaolinites by solution intercalation method. Characterization studies of PVC, kaolinite, and their nanocomposites were carried out by means of X-ray diffraction (XRD) and transmission electron microscopy (TEM); the surface areas were determined by means of NOVA 2200e BET surface area instrument; the interactions between layer silicate and PVC were determined by means of FTIR-ATR; the thermal stability was determined by means of DTA/TG; and the optical properties were determined by means of UV−vis spectrophotometer. Furthermore, the Kissinger method was used to estimate the thermal decomposition activation energy for PVC nanocomposites.

2. Material and Methods

2.1. Materials. Kaolinite and PVC, which has a molecular weight of 220 000 g/mol, were supplied from Acros Organics; tetrahydrofuran came from Riedel de Hein Chemical Co.; and dimethyl sulfoxide (DMSO) and succunimide (SIM) came from Merck Chemical Co. All other chemicals were of analytical grade, and were used without further purification. The structure of kaolinite has been given in Figure 1.[20]

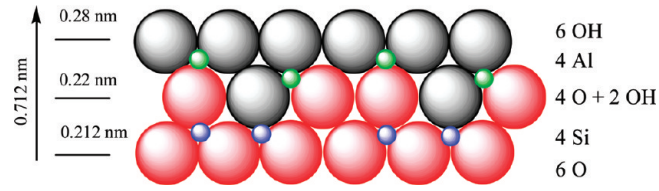

Figure 1. Crystalline structure of kaolinite, which is modified from ref 20.

2.2. Methods. 2.2.1. Modification of Kaolinite with DDMSO. Kaolinite was modified by treatment in solution with DMSO. First, kaolinite was sieved through a 50 μm sieve. Then, 5 g of sieved kaolinite and 100 mL of DMSO were added into a bottom-flask. To enhance the dispersion of kaolinite, the mixture was placed into an ultrasound field for 20 min. This suspension was stirred at 80 °C for 120 h. At last, it was filtrated and washed with methanol. This modified kaolinite was named KDMSO. KDMSO was dried at 105 °C, and then, remodified as following.[21]

2.2.2. Modification of KDMSO with SIM. SIM−KDMSO was prepared by the displacement of DMSO with SIM. The mixture of 1 g KDMSO and an aqueous solution of SIM (10% w/v, 100 mL) were stirred for 120 h at room temperature. Then, the product was filtered under vacuum, washed with 2-propanol, and dried in air.[22]

2.2.3. Nanocomposite Processing of PVC/Kaolinite Samples. For the preparation of PVC/kaolinite nanocomposites, the solution intercalation method was used. First, kaolinite in the amount of 1, 2.5, 5 wt % and 50 mL of THF was added to reaction vessels. After, these suspensions were treated in ultrasound bath for 20 min. The kaolinite suspension was stirred by magnetic stirring for 120 min. One g of PVC in 50 mL of THF was dissolved at room temperature. When PVC was completely dissolved, the kaolinite suspension was added into PVC solution flask and mixed together at room temperature for 24 h. Then, THF was evaporated at 40 °C for 24 h until PVC/kaolinite nanocomposite films were obtained. All the other procedures were the same as for kaolinite, KDMSO, and SIM−KDMSO nanocomposites.[23]

2.2.4. Thermal Degradation. Thermal degradation was done in an oven at 175 °C. Four time periods were chosen, each lasting 15 min, to investigate the level of degradation.[24]

2.3. Characterization of Nanocomposites. The nanocomposites synthesized were characterized by FTIR-ATR, XRD, TEM, BET, DTA/TG and UV−vis spectroscopy.

2.3.1. Surface Area Analysis. Surface areas of samples were analyzed by NOVA 2200e BET surface area analyzer (Quantachrome Instruments).

2.3.2. Infrared Spectroscopy. FTIR-ATR measurements were performed using a Perkin-Elmer Spectrum One Spectrometer with attenuated total reflectance (ATR). The infrared spectra were obtained in the region 4000−600 cm^{-1}.

2.3.3. X-ray Diffraction. XRD patterns of kaolinite, PVC and their nanocomposites were performed using an Analytical Philips X'Pert-Pro X-ray diffractometer equipped with a back monochromator operating at 40 kV and a copper cathode as the X-ray source (λ = 1.54 Å).

2.3.4. Thermogravimetry (DTA/TG). Thermogravimetry measurements of samples were taken using Perkin-Elmer Diamond simultaneous DTA/TG thermal analyzer at a scanning rate of 10 °C per min under nitrogen atmosphere.

2.3.5. Transmission Electron Microscopy (TEM). The characterization of samples was investigated by TEM (FEI Tecnai G2 F30). The accelerated voltage was 200 kV.

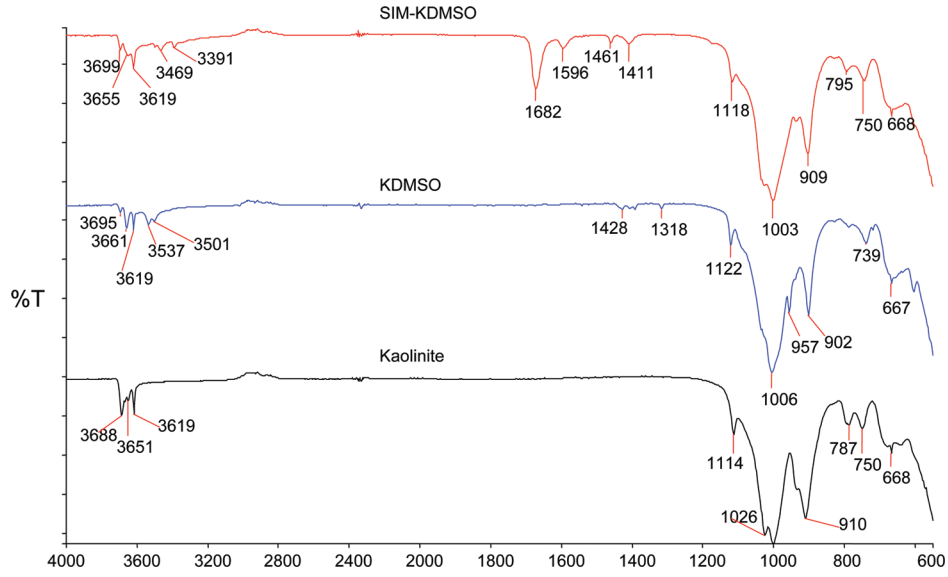

Figure 2. FTIR-ATR spectra of natural and modified kaolinites.

Table 1. Assignment of the Principle Bands of Kaolinite

wavenumbers (cm^{-1})	assignment
2688	stretching frequency of the inner-surface hydroxyl groups
3651	vibration band of adsorbed water
2619	stretching frequency of the inner hydroxyl groups
1114, 1026, and 910	Si−O stretching vibtarions
787, 750, and 668	O−Al−OH stretching vibtarions

2.3.6. UV−Visible Spectroscopy. UV−vis transmission and absorbance spectra of samples were obtained with an Perkin-Elmer Lambda 25 UV−vis spectrophotometer.

2.3.7. Thermal Kinetics. The thermogravimetric analysis was performed with Perkin-Elmer Diamond simultaneous DTA/TG thermal analyzer. Samples were heated at heating rates of 5, 10, 15, and 20 °C per min from room temperature to 600 °C under nitrogen atmosphere.

3. Results and Discussion

3.1. FTIR-ATR Characterization. There are three kinds of hydroxyl groups in kaolinite, that is, inner-surface hydroxyl, inner hydroxyl, and absorbed water hydroxyl. FTIR spectra of the hydroxyl stretch region of kaolinite are shown in Figure 2. Assignments of the principle bands of kaolinite have been given in Table 1.[25−27] Bands observed at 3688 and 3619 cm^{-1} are attributed to the phase vibration of the inner-surface hydroxyl and inner hydroxyl, respectively,[25,26] and the band at 3651 cm^{-1} is the characteristic vibration band of absorbed water. The hydroxyl group at 3619 cm^{-1} is believed to be oriented almost parallel to the direction of the (001) layers, pointing in the direction of the unoccupied octahedral hole and not usually influenced very much by interlamellar modification reactions since it is removed from the interlamellar surface. In contrast, the inner-surface hydroxyl stretching bands are very much influenced by interlamellar modifications. Other specific FTIR bands of kaolinite are due to Si−O stretching vibrations at 1114, 1026, and 910 cm^{-1} and O−Al−OH at 787, 750, and 668 cm^{-1}.[27] Because of the hydrogen-bonding between the layers, only a limited number of polar guest species such as *N*-methylformamide and DMSO can directly be intercalated. Thus, intercalation reactions of kaolinite have been extended by a guest displacement method in which new guest species can be intercalated by displacing previously intercalated species. After the intercalation of kaolinite with DMSO, the additional bands at 3537 and 3501 cm^{-1} are observed due to DMSO, the 3619 cm^{-1} vibration band of kaolinite has not been affected, while 3688 and 3651 cm^{-1} bands are affected. The bands at 3688 and 3651 cm^{-1} shifted to 3695 and 3661 cm^{-1}, respectively. The band of 3661 cm^{-1} is attributed to the hydroxyl stretching vibration of inner-surface hydroxyl groups that are hydrogen bonded to the −S═O group of DMSO. The intercalation of DMSO made intensities of 957 and 902 cm^{-1} in the fingerprint region of kaolinite descended, which is attributed to the bending vibration of the bond formed by aluminum atom and hydroxyls.

Kaolinite intercalated with DMSO was displaced by SIM using guest displacement method. As seen from Figure 2, FTIR-ATR spectra of the displacement reactions of KDMSO show definite differences from kaolinite and KDMSO spectra. The bands of KDMSO at 3537 and 3501 cm^{-1} disappeared completely, with the appearance of two bands at about 3469 and 3391 cm^{-1}. Moreover, the intensity of KDMSO band at 3661 cm^{-1} decreased. Si−O stretching vibration of kaolinite at 910 cm^{-1} remains relatively unaffected except for a small shift. In addition to this, the place or the intensity of the band at 3619 cm^{-1} has also not changed because only one of the inner-surface hydroxyl groups is H-bonded to the intercalated SIM molecules. The other clear differences that attracted attention were bands at 1682, 1596, 1461, and 1411 cm^{-1}. Infrared spectra of SIM−KDMSO show C═O peak at 1682 cm^{-1}. The intense carbonyl stretch in the spectra of SIM−KDMSO was attributed to the symmetric or antisymmetric stretching of the carbonyl groups.

Figure 3 shows FTIR-ATR spectra of PVC and PVC/kaolinite nanocomposites. Assignments of the principle bands of PVC have been given in Table 2.[28] As seen from Figure 3, FTIR spectrum of PVC showed the expected distinctive absorptions: 3200−2700 cm^{-1} (the stretching of C−H), 1500−1400 cm^{-1} (the wagging of the methylene groups), and 1331−1255 cm^{-1} (the stretching of the C−H from ClCH groups). FTIR spectrum of 2.5 wt % PVC/kaolinite nanocomposite (other results not shown in Figure) show the peaks of both PVC and kaolinite such as the peak at 1426 cm^{-1} due to the wagging of the methylene groups and those at about 1331 and 1252 cm^{-1} due to C−H deformations of CHCl. In the case of the nanocomposite, the intensity of kaolinite peaks with low kaolinite loadings has decreased. These results support that PVC/kaolinite

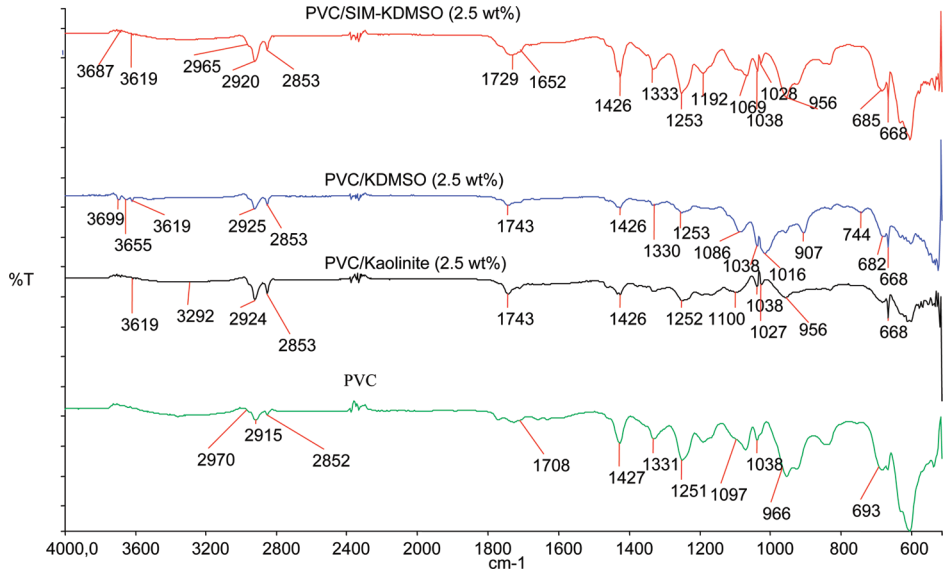

Figure 3. FTIR-ATR spectra of PVC and PVC/kaolinite nanocomposites.

Table 2. Assignment of the Principle Bands of PVC

wavenumbers (cm^{-1})	assignment
2970	stretching C−H of CHCl
2912	stretching C−H of CH_2
1435 and 1427	deformation (Wagg) CH_2
1331 and 1255	deformation C−H of CHCl
1099	stretching C−C
966	rocking CH_2
692, 637, and 616	stretching C−Cl

nanocomposites are successfully synthesized. Comparing with FTIR-ATR results in Figures 2 and 3 for KDMSO and PVC/KDMSO, it can be seen that the nanocomposite has the characteristic peaks belonging to both KDMSO and PVC. Similar results were also found for PVC/SIM−KDMSO nanocomposite. These results show that the kaolinite samples intercalated with SIM were dispersed into the PVC matrix.

3.2. XRD and TEM Characterization of Samples. The morphology of the clay-containing polymer systems is generally characterized by XRD and TEM. Low 2θ XRD enables the evaluation of the d-spacing of the intercalated structures, by evaluating how much expansion has occurred by entry of the polymer into the gallery space of the clay. Three situations are typical: (1) no change in the d-spacing and the d_{001} peak of the clay is maintained, indicating no dispersion or a microcomposite structure; (2) a peak is observed but shifted at a lower value of 2θ, which would be a classic indication of intercalated structures in the nanocomposite; (3) there can be either no d_{001} peak or a broad peak, an indicator of disorder. In the last two cases, where some dispersion occurs, one can draw no definitive conclusion about the type of dispersion, since exfoliated layers and disordered filler stacks are not detectable by XRD.[29] Figure 4 shows the XRD patterns of kaolinite and its intercalated compounds such as KDMSO and SIM−KDMSO. The XRD pattern of kaolinite has a characteristic peak at $2\theta = 12.41°$. After the intercalation of kaolinite with DMSO, the original peak of kaolinite at $2\theta = 12.41°$ has shifted to $2\theta = 7.93°$. The basal spacing (d_{001}) of KDMSO expands from 0.712 to 1.113 nm, this is an increase of 0.401 nm. The size of the S═O group is 0.338 nm, and if the DMSO parallel to the siloxane surface, then there is an imbalance of 0.063 nm. The question arises as to how this gap may be filled. In the model of the DMSO−kaolinite intercalation presented by Thomposon and Cuff,[30] one of the methyl groups is pointing directly into the ditrigonal cavity with

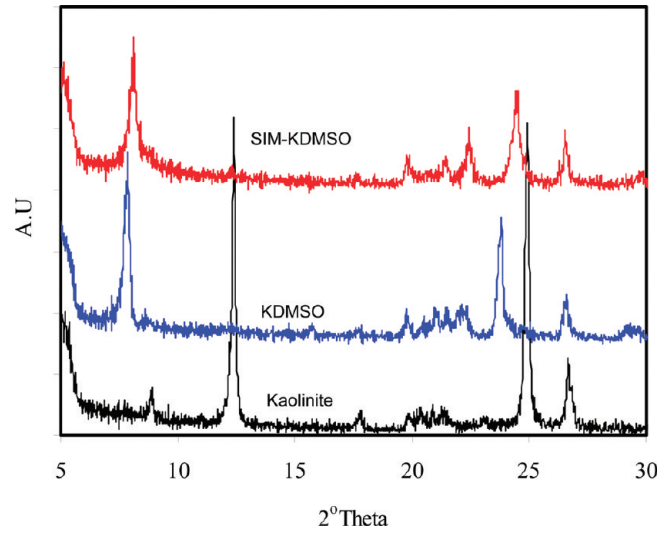

Figure 4. XRD patterns of natural and modified kaolinites.

the second methyl group pointing away from this surface. After the treatment of KDMSO intercalation compound with SIM, the basal spacing has changed from 1.113 to 1.096 nm. SIM displaced the guest molecule (DMSO), as shown by XRD patterns (see Figure 4).

The XRD traces of all of the PVC composite systems are shown in Figure 5, and no peak is seen for clay-containing compounds. PVC in the range of $2\theta = 5-30°$ has not any diffraction peak. It is an advantage to understand the composition of nanocomposite. Another significance of this situation is that PVC has an amorphous structure. Characteristic diffraction peak of kaolinite in nanocomposite case was not detected. The disappearance of the d_{001} peak of kaolinite in XRD patterns of PVC nanocomposites was considered as either an evidence for a high dispersion of kaolinite layers or a lack of orientation of the kaolinite particles within the PVC matrix. The intensity of the diffraction peak is related to the volume fraction of kaolinite, that is, the lower the volume fraction of kaolinite, the more weak the diffraction peak. These results indicate that kaolinite was dispersed in PVC matrix very well and has broken to nanoscale layers.

Again, as seen from both Figures 4 and 5, there is a peak below $2\theta = 5°$ in the XRD patterns of the PVC, kaolinite, and

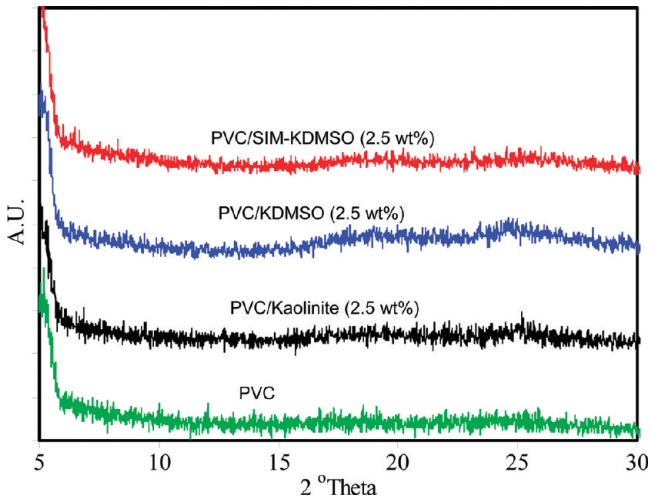

Figure 5. XRD patterns of PVC and PVC/kaolinite nanocomposites.

PVC-containing materials. This peak is due to incident very intensive X-ray beam. Since the incident X-ray beam intensity is very high, the background signal increases below that angle.

TEM enables direct imaging of the clay within the polymer, and assesses filler dispersion. TEM images of kaolinite, KDMSO, and their nanocomposites containing 1 wt % kaolinite and KDMSO have been given in Figure 6a,d. The reduction in the particle size and the associated morphological changes that occurred after intercalation reaction by DMSO of the kaolinite were clearly evident in the transmission electron micrographs. It was observed after the intercalation reaction that the original stacking layers and kaolinite booklets were delaminated and the particle size of the lamellar starting material was reduced. The usual kaolinite crystal is hexagonal or trigonal in structure and here we can see some tubiform or bar structures. TEM images of PVC/kaolinite and PVC/KDMSO nanocomposites in Figure 6c and d show that the nanocomposites have a nanomorphology. Compared with kaolinite and KDMSO, kaolinite and KDMSO in PVC matrix becomes smaller and more dispersed, and most of them were exfoliated. The combination of kaolinite and polymer seems to destroy the original structure of kaolinite and to convert the composite morphology. These results are consistent with XRD patterns.

3.3. Thermal Analysis. In practical applications, thermal properties are very important for PVC products. Figure 7 shows DTA/TG curves of kaolinite and KDMSO. DTA peak temperatures are characteristic for each mineral, and DTA curves are applicable for the identification and determination of many clays.[31] At nearly 530 °C in Figure 7a, there is an endothermic peak corresponding to the dehydroxylation of kaolinite and the formation of metakaolinite. Again, at nearly 1006 °C, an exothermic peak is related to crystallization of Al−Si spinel phase at the medium scale of temperature.[32] As seen from TG curve in Figure 7b, dehydroxylation of kaolinite results in about 11.1% mass loss. The kaolinite intercalated with DMSO exhibits two mass losses in the TG curve, accompanied with two endotherms centered at about 194 and 530 °C. The former is attributed to the loss of the organic moiety, and the latter is attributed to the usual dehydroxylation step of kaolinite. From the literature, thermogravimetric analysis of various kaolinite intercalates revealed similar results to that of KDMSO.[22] Thermogravimetric behavior could be used as a proof of the interactions between the organic medium and inorganic nanoplatelet's surface.[24] Table 3 shows T_5, T_{10}, T_{50}, and T_{80} values corresponding to 5, 10, 50, and 80 wt % weight loss of PVC film and PVC/kaolinite nanocomposites with different kaolinite loadings under nitrogen atmosphere. As seen from Table 3, the thermal stability of PVC/kaolinite nanocomposites is greater than that of pure PVC and increases as the weight fraction of kaolinite increases. A similar result was found for nanoclay PVC composites by Awad et al.[29] They investigated the thermal stability of PVC systems using a standard thermal process, evaluating the evolution of hydrogen chloride, and by color development through the yellowness index. They found that the addition of nanoclay leads to both a reduction in the total smoke that is evolved and an increase in the length of time over which smoke is evolved. It has been stated that the presence of the clay in some way interferes with the cyclization of the conjugated system formed upon HCl loss. Again, as similar to our results, many studies indicate that the nanoscale compounding of the clay particles can improve the thermal stability of polymer/MMT nanocomposites, for instance, in cases where the polymer matrices are polystyrene, poly(methyl methacrylate), and polypropylene.[33−36] The presence of MMT enhances the formation of char and hinders diffusion of volatile decomposition products within the nanocomposites.[37] In addition, the data of Table 3 show that the residue mass of PVC film is 10.02 wt % and the residue of nanocomposites increases with the increase of kaolinite content. The mass increase of residue is proportional to the kaolinite content.

Thermal gravimetric analysis (TGA) has also been used to compare the thermal decomposition of PVC and its composites, a behavior that has been shown to relate directly to the dispersion of nanoclays in a polymer matrix. Figure 8 shows derivative thermogravimetric (DTG) curves of PVC and its nanocomposites. From derivative TG curves, it can be seen that the thermal degradation of pure PVC and PVC nanocomposites occurs through two degradation steps. The temperatures at the maximum weight losses of PVC film were observed at 300 and 451 °C. The first step corresponds to the weight loss caused by the dehydrochlorination of PVC, while the second step presents the total weight loss resulted from the degradation of the dehydrochlorinated residuals. The thermal degradation temperature of PVC nanocomposites was shifted slightly to higher temperature according to pure PVC. This has shown that the existence of kaolinite in the polymer matrix prevents the degradation of PVC and organophilic treatment improves the thermal stability of PVC/clay nanocomposites, due to better interactions between PVC matrix and clay. Furthermore, this result has been supported by a second method. In this measurement method of thermal degradation, a sample is typically heated to a certain temperature and the time for HCl evolution is measured.[24] In the experiments, a heated oven was used whose temperature was set at 175 °C. Samples were put into the oven and taken out after a defined time period. It means that for the samples of each type of nanocomposites a series of time-separated thermally degraded samples were prepared. Such treated samples were then compared, see Figure 9. As can be seen from Figure 9, the temperature has an important influence on the nanocomposite's color and is different from one nanofiller to another. It is accepted that HCl originating from the dehydrochlorination of PVC chains has an autocatalytic effect on PVC thermal degradation.[38,39] As kaolinite incorporated into PVC, HCl can be absorbed by kaolinite and react with kaolinite layers. Thus, the degradation of PVC is hindered and the thermal stability of PVC composite increases. Further investigation and evaluation of the degradation were done by FTIR-ATR. Figure 10 shows FTIR-ATR spectra belonging to the degradation of PVC film under nitrogen and oxygen atmospheres. As seen in Table 2,

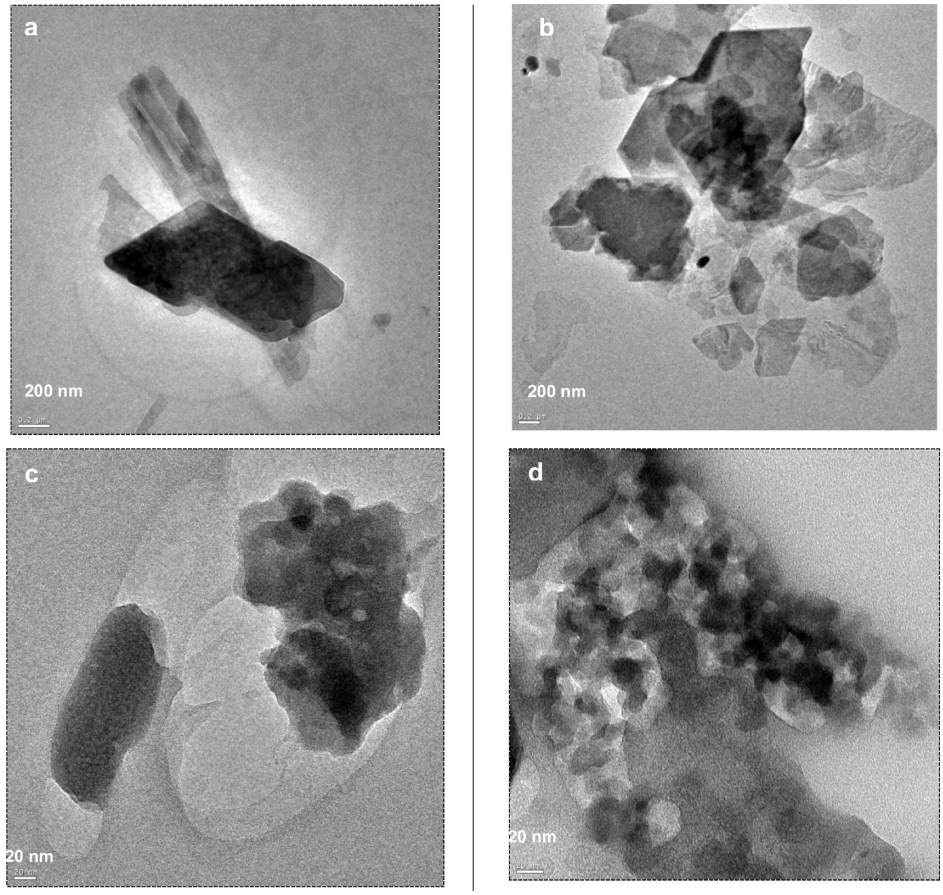

Figure 6. TEM images of (a) kaolinite, (b) KDMSO, (c) PVC/kaolinite (1 wt %), and (d) PVC/KDMSO (1 wt %).

PVC has characteristic FTIR-ATR peaks assigned to the C−Cl bond stretching vibrations in the range of 700−600 cm^{-1}; stretching C−H of CHCl in 2968 cm^{-1}; stretching C−H of CH_2 in 2912 cm^{-1}; deformation CH_2 in the range of 1435−1426 cm^{-1}; deformation C−H of CHCl at 1331−1255 cm^{-1}; stretching C−C in 1099 cm^{-1}; and rocking CH_2 in 966 cm^{-1}.[28,40] Comparing to peaks of PVC film under nitrogen and oxygen atmospheres, there are significant similarities. From the peak at about 1595 cm^{-1} for both spectra, it can be said that C═C double bonds form due to removing of HCl. The most important difference between two spectra is that the carbonyl peak at 1700 cm^{-1} in the spectrum under nitrogen atmosphere disappeared. During oxidative processing, in addition to thermal dehydrochlorination, the polymer is exposed to thermo-oxidative degradation resulting from oxygen. The main feature in thermo-oxidative degradation is dehydrochlorination as in thermal degradation. The presence of oxygen causes the dehydrochlorination process to accelerate, but the discoloration is not as severe as during thermal degradation. The degradation reaction of PVC under nitrogen can be written as following:

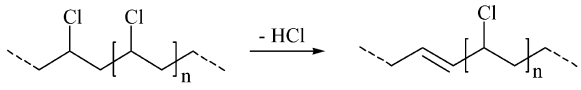

[1]

From Table 3, the temperatures corresponding to 5, 10, 50, and 80 wt % weight loss increase from 135 to 153 °C, from 151 to 258 °C, from 313 to 326 °C and from 456 to 476 °C for pure PVC and PVC/KDMSO with 2.5 wt % KDMSO loading, respectively. From Table 3 the values for PVC/SIM−KDMSO (2.5%) are lower than for PVC/KDMSO (2.5%) but higher than the values for PVC/kaolinite (2.5%). Moreover, the formation of residue was noticeably increased from pure PVC to the nanocomposites. Table 4 shows the specifice surface areas of samples. The specific surface areas of modified kaolinite samples are higher than that of natural kaolinite. Another reason for an increase in the thermal stability of PVC may be that the specific surface area of the clay interlayer surface is much larger than the outside surface, and PVC in the clay interlayer surface has a stronger interaction, with the two-dimensional clay interlayer constraining the segmental motion of interlayer PVC.[41] In studies on thermal stability of PVC nanocomposites with layered silicates, the presence of the quaternary ammonium in the nanocomposites was found to be responsible for the acceleration of the polymer decomposition. The quaternary ammonium salt decomposed following the Hofmann degradation mechanism. It was previously proved that the presence of H^+ and HCl may (auto)catalyze the dehydrochlorination of the PVC chains.[42]

3.4. Kinetics of Thermal Degradation. Kinetic study of thermal degradation provides useful information for the optimization of the successive treatment of polymer materials in order to avoid or at least limit thermal degradation. The analysis of the degradation process becomes more and more important due to an increase in the range of temperatures for engineering applications, recycling of postconsumer plastic waste, as well as the use of polymers as biological implants and matrices for drug delivery, where depolymerization is an inevitable process affecting the lifetime of an article.[43] Degradation kinetics was extensively investigated by thermogravimetry analysis. Thermal degradation of PVC and PVC/kaolinite nanocomposite with 5 wt % loading were studied by determination of their mass loss during heating. TG curves of PVC and its nanocomposite for first and second stages under nitrogen atmosphere at various

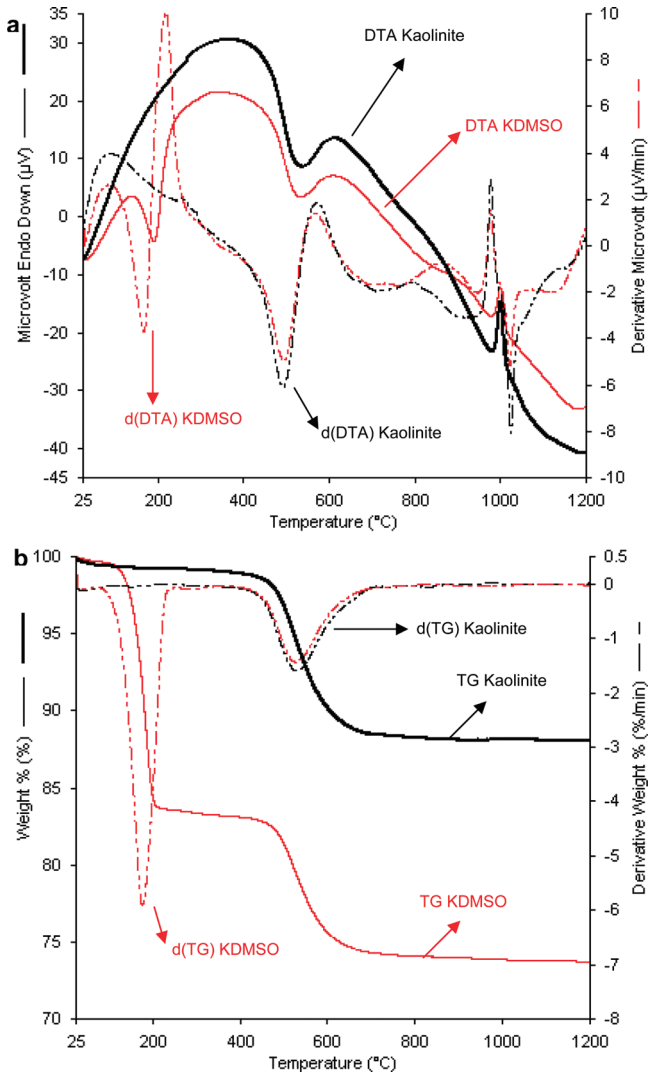

Figure 7. (a) DTA and (b) TG plots of kaolinite and KDMSO samples.

Table 3. Thermal Stability Parameters of PVC and Its Nanocomposites

samples	T_5 (°C)	T_{10} (°C)	T_{50} (°C)	T_{80} (°C)	residue (%)
PVC	135	151	313	456	10.02
PVC/kaolinite (1 wt %)	143	159	313	461	12.22
PVC/kaolinite (2.5 wt %)	139	155	316	464	12.36
PVC/kaolinite (5 wt %)	132	152	315	472	14.55
PVC/KDMSO (1 wt %)	147	255	325	473	12.72
PVC/KDMSO (2.5 wt %)	153	258	326	476	13.94
PVC/KDMSO (5 wt %)	150	245	327	488	15.91
PVC/SIM−KDMSO (2.5 wt %)	148	190	318	478	13.59

heating rates (5, 10, 15, and 20 °C/min) are shown in Figure 11a,b. All curves are approximately the same shape. TG curves of PVC and its nanocomposite show two stages of mass loss. The degradation trend of PVC/kaolinite nanocomposite is similar to that of pure PVC under the nitrogen environment. The presence of the nanoparticles caused a shift of the mass loss temperature to higher temperatures.

Several equations to indicate kinetic parameters of the degradation of polymeric materials are known. The Kissinger method has been used in the literature to determine the activation energy from plots of the logarithm of the heating rate versus the inverse of the temperature at the maximum reaction rate in constant heating rate experiments.[44] The activation energy can

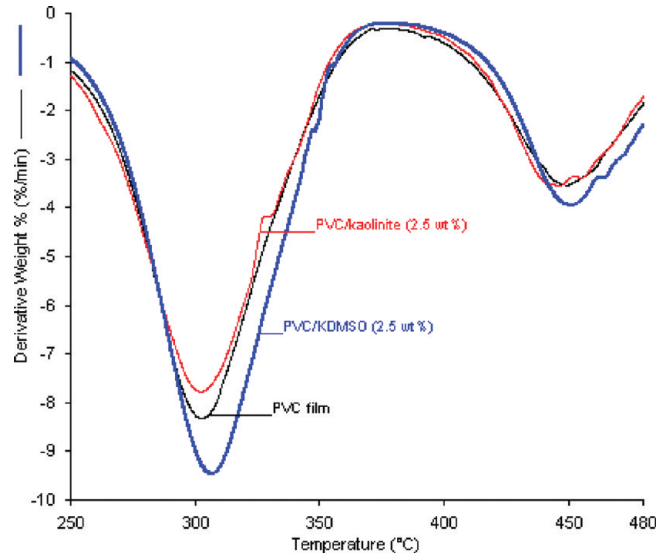

Figure 8. Derivative thermogravimetric (DTG) curves of PVC and its nanocomposites.

be determined by the Kissinger method without a precise knowledge of the reaction mechanism, using the equation

$$\ln\left(\frac{\beta}{T_{max}^{2}}\right) = -\frac{E_a}{RT_{max}} + \left\{\ln\frac{AR}{E_a} + \ln[n(1-\alpha_{max})^{n-1}]\right\} \quad (2)$$

where β is the heating rate; T_{max} is the temperature corresponding to the inflection point of the thermal degradation curves which corresponds to the maximum reaction rate; A is the pre-exponential factor; E_a is the activation energy; α_{max} is the maximum conversion and n is the order of the reaction. From a plot of $\ln(\beta/T_{max}^2)$ versus $1/T_{max}$, and fitting to a straight line, the activation energy E_a can be calculated from the slope. TG data of PVC and PVC/kaolinite obtained under nitrogen atmosphere at different heating rates have been given in Table 5. Figure 12 shows the relationship given by eq 2, known as Kissinger technique, $\ln(\beta/T_{max}^2)$ vs $(1/T_{max})$]. The kinetic parameters for thermal degradation are calculated considering the heating rates of 5, 10, 15, and 20 °C/min, and the results are summarized in Table 6. The results show that activation energy values at both stages for PVC/kaolinite nanocomposite are higher than those of pure PVC, indicating that addition of kaolinite particles improves thermal stability of PVC.

3.5. Optical Properties. In general, microsized particles used as reinforcing agents scatter light, thus reducing light transmittance and optical clarity.[45] In nanocomposites, the domain sizes are reduced to a level such that true molecular composites are formed. As a result of this intimate mixing, these hybrids are often highly transparent, a property which renders them amenable to applications outside the boundaries of traditional composites. In this study, PVC film and its nanocomposite films were used for optical measurements. Figure 13a presents the UV−vis transmission spectra in the region of 190−600 of PVC film and its nanocomposites with 1−5 wt % kaolinite. These spectra are affected by the presence of the clay in PVC matrix. However, the spectra of films at higher kaolinite loading exhibit lower optical clarity, indicating that there is a strong scattering of kaolinite resulting in lower transparency of the UV light. Figure 13b shows the UV−vis transmission spectra of PVC, PVC/KDMSO, and PVC/SIM−KDMSO. In this graph, there is a

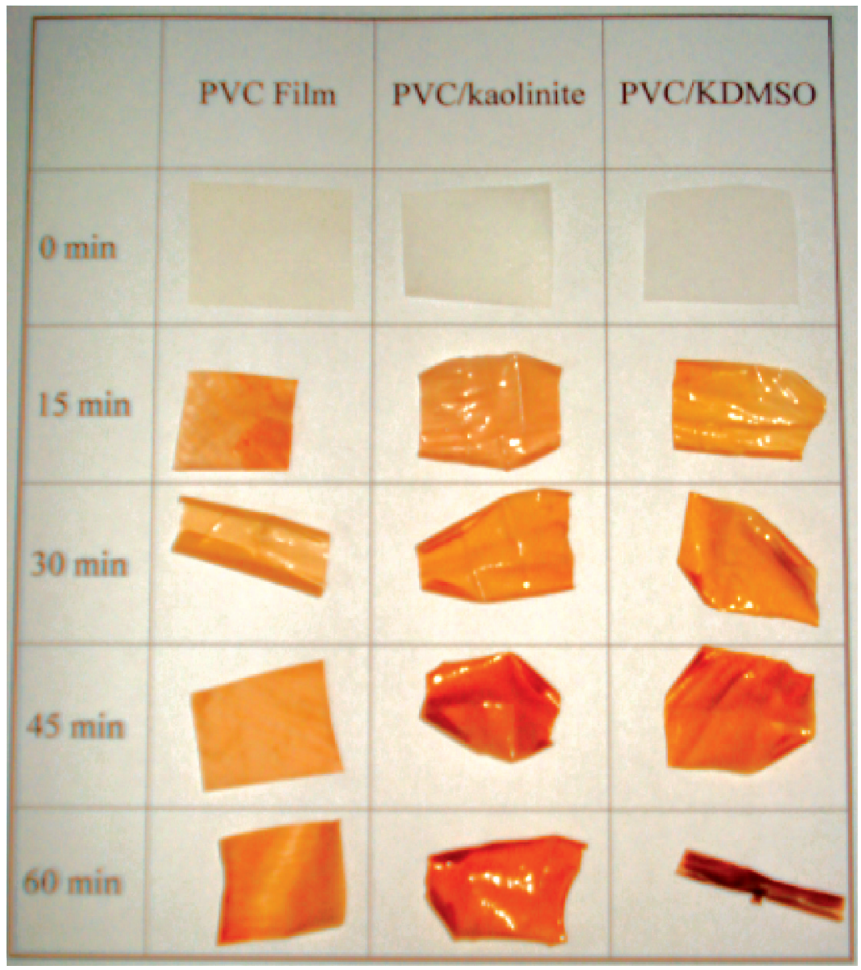

Figure 9. Color changes in nanocomposites after thermal degradation.

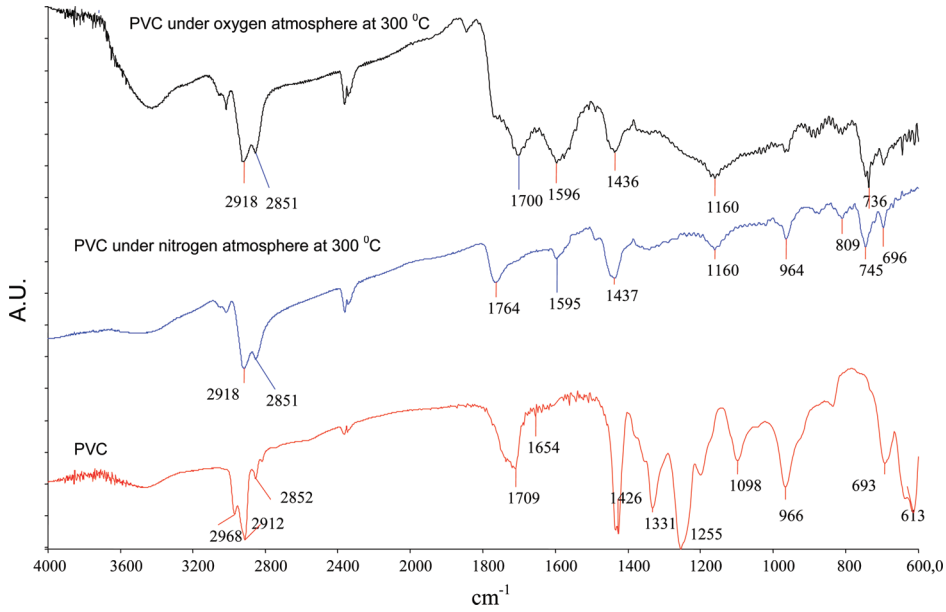

Figure 10. FTIR-ATR analysis for thermal degradation of PVC.

broad peak in the UV region. This peak is originated from DMSO. Again, as seen from Figure 13b, PVC/SIM−KDMSO nanocomposite has higher UV transmission than pure PVC but it has lower UV transmission than other nanocomposites. At the same time, this graph verifies the insertion of DMSO between clay layers and substitution of DMSO with SIM by

Table 4. BET Surface Areas of Kaolinite and Modified Kaolinite Samples

samples	surface area (m^2/g)
kaolinite	8.8
KDMSO	21.7
SIM−KDMSO	25.5

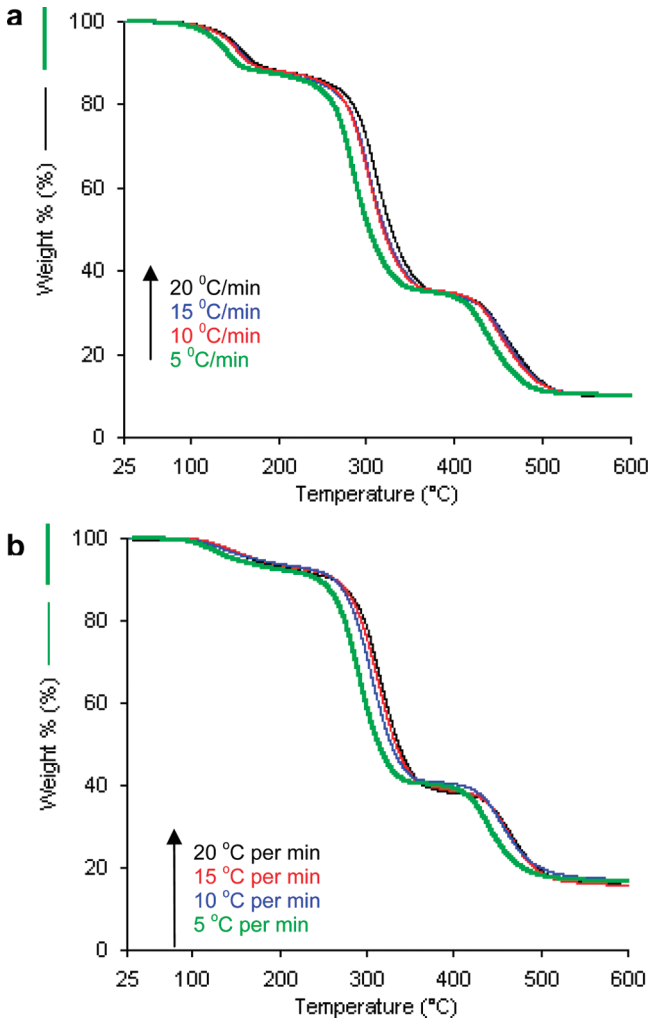

Figure 11. TG curves of (a) PVC and (b) PVC/kaolinite nanocomposite with 5 wt % clay loadings at different heating rates under nitrogen atmosphere.

Table 5. TG Data of PVC and PVC/Kaolinite Obtained under Nitrogen Atmosphere at Different Heating Rates

samples	heating rates (°C/min)	$T_{10\%}$ (°C)	$T_{50\%}$ (°C)	T_{max1} (°C)	T_{max2} (°C)	residue at 600 °C
PVC	5	153	303	283	434	10.02
	10	167	318	300	451	10.22
	15	169	320	300	458	10.23
	20	174	327	311	456	9.81
PVC/kaolinite	5	243	314	293	442	16.60
	10	262	328	305	459	17.15
	15	263	336	314	461	16.71
	>20	271	340	319	464	16.96

guest displacement reaction because the broad peak in PVC/KDMSO spectra has disappeared in PVC/SIM−KDMSO spectra. As seen in Figure 13a,b, PVC/kaolinite nanocomposites have a lower UV transmission than PVC/KDMSO nanocomposites when they have the same clay content. This should be tied back to the better dispersion, and lower particle size (as seen in the TEM pictures). As a result, it can be said that the nanocomposites obtained have better optical transparency than that of PVC film. A similar result was obtained by Li et al. for PMMA-kaolinite nanocomposite films.[46]

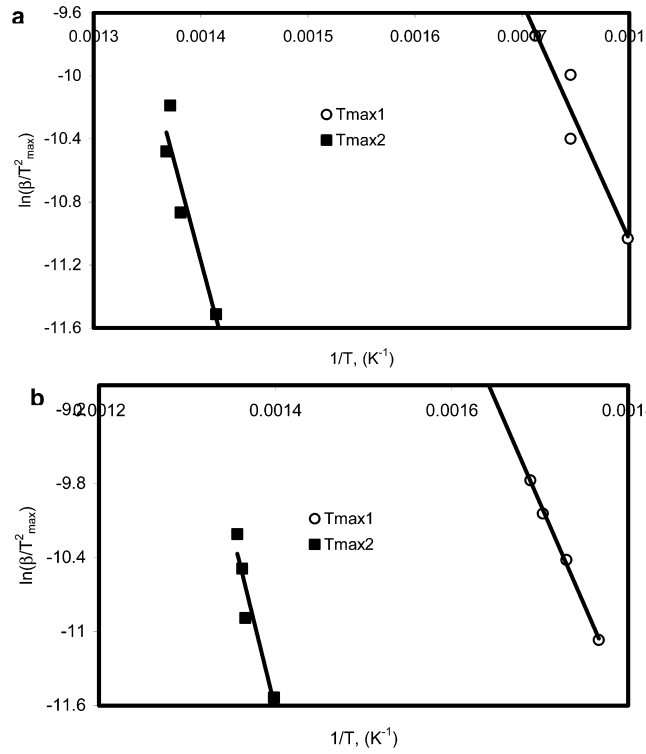

Figure 12. The plots used for the determination of the activation energies of (a) pure PVC and (b) PVC/kaolinite samples consisting of 5 wt % kaolinite according to the Kissinger's method.

Table 6. Activation Energies of PVC and PVC/Kaolinite Samples by Kissinger Method

samples at different stages	slope	E_a (kJ/mol)	R^2
PVC at the first stage degradation	−14547	125	0.997
PVC at the second stage degradation	−25439	211	0.882
PVC/kaolinite at the first stage degradation	−16460	136	0.997
PVC/ kaolinite at the second stage degradation	−29143	242	0.907

4. Conclusions

A series of nanocomposite materials consisting of PVC and layered kaolinite clay were prepared by effectively dispersing of the inorganic nanolayers of kaolinite clay in PVC matrix by the solution intercalation method. FTIR-ATR, XRD, TEM, DTA/TG, BET, and UV−vis spectrophotometer experiments were carried out to characterize the morphology and properties of the nanocomposites. By means of intercalation of kaolinite with DMSO, the basal spacing of a natural kaolinite expanded from 0.712 to 1.113 nm. It has also been observed that the organophilicity of kaolinite was enhanced. The intercalation of KDMSO with SIM are intercalated in the interlayer spaces of kaolinite by guest-displacement method. Evidence from several spectroscopic and thermal analysis shows that SIM replaces the DMSO molecules. The incorporation of nanoparticle with polymer results in an increase in thermal stability. The nanocomposites enhance the formation of residue and improve the thermal stability of the polymer matrix. The intercalated composites exhibit bigger UV transparency, but this transparency decreases with increase in kaolinite amount. Comparing values for the activation energies for the thermal degradation of PVC and PVC/kaolinite via the Kissinger method, we find that there is an obvious trend for the increase of the apparent activation energy of the nanocomposite. This increasing trend

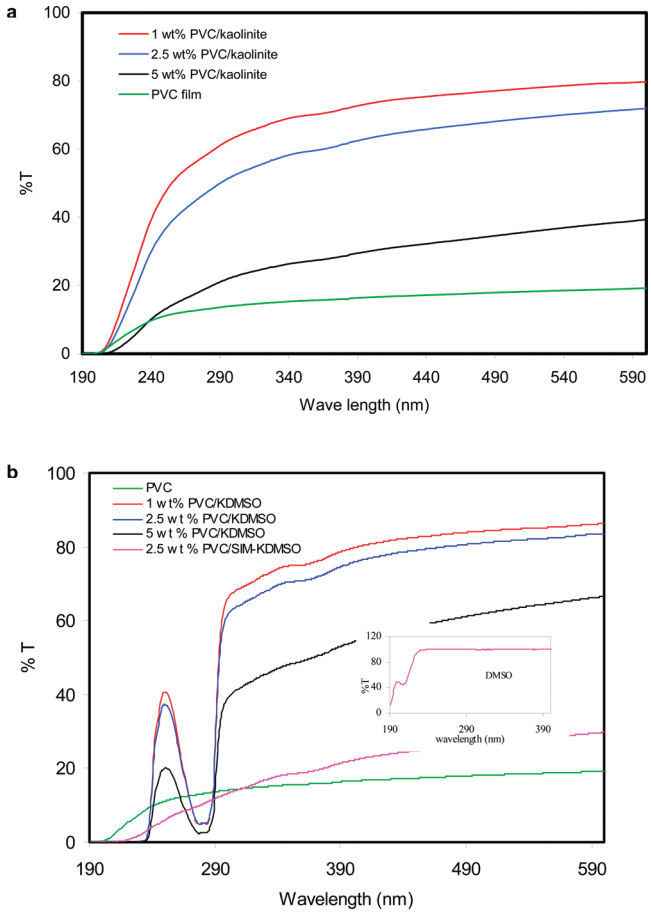

Figure 13. The UV−vis transmittance spectra of (a) PVC/kaolinite and (b) PVC/KDMSO nanocomposites.

coincides with the thermal analysis results that the polymer/clay nanocomposite has a higher thermal stability.

Acknowledgment

The work was financially supported by Balikesir University Research Fund (Project 2008/20).

Literature Cited

(1) Ishida, H.; Campbell, S.; Blackwell, J. General approach to nanocomposite preparation. *Chem. Mater.* **2000**, *12* (5), 1260–1267.

(2) Giannelis, E. P. Polymer layered silicate nanocomposites. *Adv. Mater.* **1996**, *8* (1), 29–35.

(3) Pinnavaia, T. J.; Beall, G. W. *Polymer-Clay Nanocomposites*; Wiley Series in Polymer Science; Wiley: Chichester, U.K. 2000.

(4) Viville, P.; Lazzaroni, R.; Pollet, E.; Alexandre, M.; Dubois, P.; Borcia, G.; Pireaux, J.-J. Surface characterization of poly(ϵ-caprolactone)-based nanocomposites. *Langmuir* **2003**, *19*, 9425–9433.

(5) Alexandre, M.; Dubois, P. Polymer-layered silicate nanocomposites: Preparation, properties, and uses of a new class of materials. *Mater. Sci. Eng.* **2000**, *28* (1−2), 1–63.

(6) Jang, B. N.; Wang, D.; Wilkie, C. A. Relationship between the solubility parameter of polymers and the clay dispersion in polymer/clay nanocomposites and the role of the surfactant. *Macromolecules* **2005**, *38* (15), 6533–6543.

(7) Okada, A.; Kawasumi, M.; Kurauchi, T.; Kamigaito, O. *Abstr. Pap. Am. Chem. Soc.* **1987**, *194*, 10.

(8) Benlikaya, R.; Alkan, M.; Kaya, I. Preparation and characterization of sepiolite-poly(ethyl methacrylate) and poly(2-hydroxyethyl methacrylate) nanocomposites. *Polym. Compos.* DOI: 10.1002/pc.20731.

(9) Giese, R. F. The electrostatic interlayer forces of layer structure minerals. *Clays Clay Mineral.* **1978**, *26* (1), 51–57.

(10) Liang, L.; Liu, J.; Gong, X. Thermosensitive poly(*N*-isopropylacrylamide)-clay nanocomposites with enhanced temperature response. *Langmuir* **2000**, *16* (25), 9895–9899.

(11) Chen, N.; Wan, C.; Zhang, Y.; Zhang, C. Fracture behavior of PVC/Blendex/nano-$CaCO_3$ composites. *J. Appl. Polym. Sci.* **2005**, *95* (4), 953–961.

(12) Chen, G.; Tian, M.; Guo, S. A study on the morphology and mechanical properties of PVC/nano-SiO_2 composites. *J. Macromol. Sci., Part B* **2006**, *45*, 709.

(13) Zhu, A.; Shi, Z.; Cai, A.; Zhao, F.; Liao, T. Synthesis of core-shell PMMA-SiO_2 nanoparticles with suspension−dispersion−polymerization in an aqueous system and its effect on mechanical properties of PVC composites. *Polym. Test.* **2008**, *27* (5), 540–547.

(14) Wan, C. Y.; Qiao, X. Y.; Zhang, Y.; Zhang, Y. X. Effect of different clay treatment on morphology and mechanical properties of PVC-clay nanocomposites. *Polym Test.* **2003**, *22* (4), 453–461.

(15) Vandevyver, E.; Eichholz, E. Latest advancements in PVC/clay nanocomposites: Potential applications in plastisols. *Plast. Rubber Compos.* **2008**, *37*, 417–420.

(16) Wang, D. Y.; Parlow, D.; Yao, Q.; Wilkie, C. A. PVC−clay nanocomposites: Preparation, thermal and mechanical properties. *J. Vinyl Addit. Technol.* **2002**, *7* (4), 203–213.

(17) Wang, D. Y.; Parlow, D.; Yao, Q.; Wilkie, C. A. Melt blending preparation of PVC−sodium clay nanocomposites. *J. Vinyl Addit. Technol.* **2002**, *8* (2), 139–150.

(18) Du, J. X.; Wang, D. Y.; Wilkie, C. A.; Wang, J. Q. An XPS investigation of thermal degradation and charring on poly(vinyl chloride)-clay nanocomposites. *Polym. Degrad. Stab.* **2003**, *79* (2), 319–324.

(19) Alkan, M.; Demirbaş, Ö.; Doğan, M. Electrokinetic properties of kaolinite in mono- and multivalent electrolyte solutions. *Microporous Mesoporous Mater.* **2005**, *83* (1−3), 51–59.

(20) Greenwood, N. N.; Earnshaw, A. *Chemistry of the Elements*; Pergamon: U.K., 1984.

(21) Cabeda, L.; Gimenez, E.; Lagoron, J. M.; Gavara, R.; Saura, J. J. Development of EVOH−kaolinite nanocomposites. *Polymer.* **2004**, *45* (15), 5233–5238.

(22) Elbokl, T. A.; Detellier, C. Intercalation of cyclic imides in kaolinite. *J. Colloid Interface Sci.* **2008**, *323* (2), 338–348.

(23) Chen, W.; Feng, L.; Qu, B. In situ synthesis of poly(methyl methacrylate)/MgAl layered double hydroxide nanocomposite with high transparency and enhanced thermal properties. *Solid State Commun.* **2004**, *130* (3−4), 259–263.

(24) Peprnick, T.; Duchet, J.; Kovarova, L.; Malac, J.; Gerard, J. F.; Simonik, J. Poly(vinyl chloride)/clay nanocomposites: X-ray diffraction, thermal and rheological behaviour. *Polym. Degrad. Stab.* **2006**, *91*, 1855–1860.

(25) Ledoux, R. L.; White, J. L. J. Infrared studies of hydrogen bonding interaction between kaolinite surfaces and intercalated potassium acetate, hydrazine, formamide, and urea. *J. Colloid Interface Sci.* **1996**, *21* (2), 127–152.

(26) Van der Marel, H. W.; Beutelspacher, H. *Atlas of Infrared Spectroscope of Clay Minerals and Their Admixtures*; Elsevier: Amsterdam, The Netherlands, 1976.

(27) Zhang, B.; Li, Y.; Pan, X.; Jia, X.; Wang, X. Intercalation of acrylic acid and sodium acrylate into kaolinite and their in situ polymerization. *J. Phys. Chem. Solids.* **2007**, *68* (2), 135–142.

(28) Beltran, M.; Marcilla, M. Fourier transform infrared spectroscopy applied to the use of PVC decomposition. *Eur. Polym. J.* **1997**, *33* (7), 1135–1142.

(29) Awad, W. H.; Beyer, G.; Benderly, D.; Ijdo, W. L.; Songtipya, P.; Jimenez-Gasco, M. M.; Manias, E.; Wilkie, C. A. Material properties of nanoclay PVC composites. *Polymer* **2009**, *50*, 1857–1867.

(30) Tomposon, J. G.; Cuff, C. Crystal structure kaolinite: dimethyl sulfoxide intercalate. *Clay Clay Miner.* **1985**, *33*, 490–500.

(31) Karaoglu, M. H.; Doğan, M.; Alkan, M. Removal of cationic dyes by kaolinite. *Microporous Mesoporous Mater.* **2009**, *122* (1−3), 20–27.

(32) Alkan, M.; Kalay, B.; Doğan, M.; Demirbas, O. Removal of copper ions from aqueous solutions by kaolinite and batch design. *J. Hazard. Mater.* **2008**, *153* (1−2), 867–876.

(33) Chen, G. M.; Liu, S. H.; Chen, S. J.; Qi, Z. N. FTIR spectra, thermal properties, and dispersibility of a polystyrene/montmorillonite nanocomposite. *Macromol. Chem. Phys.* **2001**, *202*, 1189–1193.

(34) Blumstein, A. Polymerization of absorbed monolayers P. Thermal degradation of the inserted polymer. *J. Polym. Sci., Part A* **1965**, *3*, 2665.

(35) Zhu, J.; Start, P.; Mauritz, K. A.; Wilkie, C. A. Thermal stability and flame retardancy of poly(methyl methacrylate)eclay nanocomposites. *Polym. Degrad. Stab.* **2002**, *77*, 253.

(36) Zanetti, M.; Camino, G.; Peichert, P.; Mulhaupt, R. Thermal behavior of poly(propylene) layered silicate nanocomposites. *Macromol. Rapid Commun.* **2001**, *22*, 176.

(37) Gong, F.; Feng, M.; Zhao, C.; Zhang, S.; Yang, M. Thermal properties of poly(vinyl chloride)/montmorillonite nanocomposites. *Polym. Degrad. Stab.* **2004**, *84*, 289.

(38) Starnes, W. H., Jr. Structural and mechanistic aspects of the thermal degradation of poly(vinyl chloride). *Prog. Polym. Sci.* **2002**, *27* (10), 2133–2170.

(39) Bao, Y.-Z.; Huang, Z.-M.; Li, S.-X.; Weng, Z.-X. Thermal stability, smoke emission and mechanical properties of poly(vinyl chloride)/hydrotalcite nanocomposites. *Polym. Degrad. Stab.* **2008**, *93* (2), 448–455.

(40) Leszczynska, A.; Njuguna, J.; Pielichowski, K.; Banerjee, J. R. Polymer/montmorillonite nanocomposites with improved thermal properties: Part II. Thermal stability of montmorillonite nanocomposites based on different polymeric matrixes. *Thermochim. Acta* **2007**, *454* (1), 1–22.

(41) Chen, Z.; Huang, C.; Liu, S.; Zhang, Y.; Gong, K. Synthesis, characterization and properties of clay−polyacrylate hybrid materials. *J. Appl. Polym. Sci.* **2000**, *75* (6), 796–801.

(42) Scott, G.; Tahan, M. Effect of some additives on the photoxidation of rigid PVC. *Eur. Polym. J.* **1975**, *11* (7), 535–539.

(43) Pielichowski, K.; Njuguna, J. *Thermal Degradation of Polymeric Materials*; Rapra Technology Limited Shawbury: Shrewsbury, U.K., 2005.

(44) Dong, Q. X.; Chen, Q. J.; Yang, W.; Zheng, Y. L.; Liu, X.; Li, Y. L.; Yang, M. B. Thermal properties and flame retardancy of polycarbonate/hydroxyapatite nanocomposite. *J. Appl. Polym. Sci.* **2008**, *109*, 659–663.

(45) Schmidt, G.; Malwitz, M. M. Properties of polymer−nanoparticle composites. *Curr. Opin. Colloid Interface Sci.* **2003**, *8* (1), 103–108.

(46) Li, Y.; Zhang, B.; Pan, X. Preparation and characterization of PMMA−kaolinite intercalation composites. *Compos. Sci. Technol.* **2008**, *68* (9), 1954–1961.

Received for review September 3, 2009
Revised manuscript received December 3, 2009
Accepted December 19, 2009

IE901384X